Furin sustains tumor-promoting signals in KRAS- and BRAF-mutated colorectal cancer by engaging the TGF-β1–COX-2 axis in a reciprocal regulatory network

Abdel-Majid Khatib

majid.Khatib@inserm.fr

INSERM BRIC U1312 https://orcid.org/0000-0001-6957-0384

Yiyang Liu

INSERM BRIC U1312

Geraldine Siegfried

Zongsheng He

INSERM BRIC U1312

Sabine Tejpar

University Hospital Gasthuisberg, 3000 Leuven, Belgium

Torsten Steinmetzer

John Creemers

KU Leuven https://orcid.org/0000-0003-2518-9295

Article

Keywords:

Posted Date: October 27th, 2025

DOI: https://doi.org/10.21203/rs.3.rs-7633807/v1

Additional Declarations: There is **NO** conflict of interest to disclose.

Abstract

KRAS and BRAF mutations drive colorectal cancer (CRC) progression by sustaining aberrant signaling and promoting therapeutic resistance. Here, we identify TGF-β1-COX-2 axis as a critical regulatory pathway mediated by Furin in CRC harboring KRAS or BRAF mutation. Genetic silencing or pharmacological inhibition of Furin in KRAS-mutant (KPN) and BRAF-mutant (BPN) tumor-derived cells suppressed tumor growth, reduced angiogenesis, and enhanced $CD8^+$ T cell infiltration in mouse tumor models. KRAS- and BRAF-mutant organoids with impaired Furin activity exhibited increased sensitivity to 5-FU, oxaliplatin, and irinotecan. Mechanistically, Furin inhibition via shRNA or the Furin inhibitor MI1148 blocked IGF-1 receptor and TGF-β1 precursor maturation and signaling, which was associated with repressed COX-2 expression. Conversely, COX-2 over-expression elevated TGF-β1 levels, which in turn enhanced Furin expression, establishing a feed-forward loop that promoted tumor progression and angiogenesis. Moreover, Furin inhibition largely disrupted the activity of multiple kinases linked to KRAS and BRAF oncogenic signaling. In CRC patient samples, Furin expression positively correlated with KRAS, BRAF, TGF-β1, and COX-2. Collectively, these findings identify Furin as a pivotal regulator of oncogenic signaling in KRAS- and BRAF-mutant CRC, and highlight the therapeutic potential of targeting the Furin-TGF-β1-COX-2 axis.

Introduction

Colorectal cancer (CRC) is one of the most prevalent malignancies of the digestive system and is the second leading cause of cancer-related mortality worldwide [1]. Although the exact etiology is not always clear, genetic factors, aging, and lifestyle significantly increase the risk of CRC development [2]. In recent years, experimental and clinical studies have revealed that multiple signaling (over) activation initiates or promotes the progression of CRC [3–5], particularly the MAPK, PI3K, WNT, and COX-2 signaling pathways [3,6]. Pharmacological inhibition of these pathways has become a widely used approach to prolong overall survival of patients with CRC [6]. However, these inhibitory strategies are not always effective because of gene mutations in the related signaling pathways. For example, cetuximab, an antibody that targets epidermal growth factor receptor (EGFR), can slow CRC progression in the clinic by inhibiting EGFR-mediated activation of the MAPK and PI3K pathways [7,8]. Nonetheless, as with other therapies, the effectiveness of cetuximab is limited across different patient populations [9].

Resistance to treatment has been linked to the presence of KRAS and BRAF mutations in CRC [10–12]. Indeed, 40% of CRC tumors exhibit activating mutations in KRAS (e.g., G12D, G13D, and Q61H), leading to the continuous activation of KRAS [13]. This mutant KRAS functions as a molecular switch, persistently triggering downstream RAF/MEK/ERK and PI3K/AKT signaling, which promotes cell proliferation and survival, thereby contributing to tumorigenesis and resistance to therapy [14,15]. Although BRAF mutations are less common than KRAS mutations in CRC (occurring in approximately 8–12% of cases [16]), these mutations, such as the classic V600E mutation, lead to more aggressive tumor behavior [17], and BRAF mutations are often linked to poor responses to chemotherapy, shorter progression-free survival, and

reduced overall survival [18]. Despite these insights, the development of effective targeted drugs for KRAS and BRAF mutations remains a significant challenge [10,19,20]. Therefore, understanding the molecular complexities of the progression of this CRC subtype is crucial for the development of more effective targeted therapies and personalized treatment strategies that can interfere with the KRAS and/or BRAF mutation activity in cancer cells.

Furin, together with other members of the proprotein convertase (PC) family (PC1/3, PC2, PC4, PACE4, PC5/6, and PC7), cleaves proproteins with basic motifs, such as Arg-X-Lys/Arg-Arg [21–23]. Within this family, PC1/3, PC2, and PC4 exhibit tissue-specific distribution, whereas Furin is expressed in a broad range of cell lines and tissues. In a steady state, Furin predominantly localizes within the trans-Golgi network, where it engages in a dynamic cycling process involving the sorting compartment, cell surface, and early endosomes [24]. Owing to its ubiquitous expression, Furin has been suggested to cleave more than 100 substrates, ranging from growth factors and their receptors to adhesion molecules and extracellular matrix proteins, although only a few have been confirmed *in vivo* [21,25–27]. Many of these protein precursors are involved in initiating and sustaining cancer hallmarks [21,22,28], suggesting that Furin is a promising target for therapeutic intervention in various human cancers [21,23,29]. Using mouse-derived KRAS-mutant colorectal cancer (CRC) cell lines and organoids (KPN: villinCre^{ER} Kras$^{G12D/+}$; Trp53$^{fl/fl}$; Rosa26$^{N1icd/+}$) and BRAF-mutated CRC cell line and organoids (BPN: villinCre^{ER} BRAF$^{V600E/+}$; Trp53$^{fl/fl}$; Rosa26$^{N1icd/+}$), we found that Furin repression enhanced the sensitivity of both KRAS- and BRAF-mutant CRC models to standard chemotherapeutic agents. In these CRC models, Furin regulates cyclooxygenase-2 (COX-2) expression through the proteolytic activation of TGF-β1 and its downstream signaling, both in vitro and in vivo. These findings suggest that targeting the Furin-TGF-β1-COX-2 interaction may represent a promising therapeutic strategy for KRAS- and/or BRAF-mutant colorectal cancer, potentially addressing a critical unmet need in this aggressive disease subtype.

Materials and Methods

Human tumor samples

Samples from 25 colorectal cancer patients (both male and female) and adjacent normal regions were collected from frozen tissues. The specimens were clinically and histopathologically diagnosed at the Institut Bergonié, Bordeaux. The tissues acquired after resection were promptly placed on ice post-surgery and snap-frozen in liquid nitrogen for subsequent analysis. For human experiments, ethics approval was obtained from the Bergonié Institute, key projects [PV2024_071]). Patient consent forms were obtained for all samples at the time of tissue acquisition. The biopsies were de-identified.

Plasmids and lentiviral transduction

The plasmid encoding pLenti-shFurin was generated by amplifying the corresponding cDNA via PCR (shRNA-Furin; Sigma; 11042118MN; forward primer: CGCGAGTCTAGAATGGAGCTGAGGCCCTGG;

reverse primer: CGAGTTGTCGACTCAGAGGGCGCTCTGGTC) and ligating the Xbal/Sal1-digested PCR product into Xbal/Sal1-restricted pLenti CMV GFP Puro (Addgene; 17448). The plasmid encoding pLenti-PTGS2 was generated by amplifying the corresponding cDNA via PCR (template: pcDNA3.1-hPTGS2-2flag; addgene;102498; forward primer: CGATGGGATCCACCATGCTCGCCCGCGCC; reverse primer: CGACTTGTCGACCTACAGTTCAGTCGAACGTTC), and the BamHI/Sal1-digested PCR product was ligated into the BamHI/Sal1-restricted pLenti CMV GFP Puro (Addgene;17448). The DH5α coli strain (Thermo Fisher Scientific) was used as the cloning and plasmid amplification host. All plasmids were validated using DNA sequencing (LGC Genomics, Berlin, Germany). To produce lentiviral particles, HEK-293T cells were incubated in DMEM/F12 medium and co-transfected with 1 µg/µL pLenti-shFurin/pLenti-COX-2 construct, 1 µg/µL p-VSVG construct (Addgene; 8454), or 1 µg/µL delta 8.91 (Addgene; 12247) with 7 µL XtremeGene9 transfection reagent (41106502, Sigma). The medium was aspirated after 6 h and replaced with fresh DMEM/F12 supplemented with 10% FCS. The supernatant was harvested after 48 h, centrifuged at 1000 × g at 4°C for 10 min, filtered through a 0.4 µm low protein-binding membrane (UFC905024, Millipore), and used to infect CRC cells in the presence of 8 mg/mL polybrene (107689, Sigma). The virus-containing media were removed 48 h after transduction, and the infected cells were selected with 2 µg/mL puromycin for 7 days (P7255, Sigma).

Cell culture, organoid generation, and cell transfection

The characteristics of the KRAS- and BRAF-mutated cancer mouse models, in which KPN cells harboring KRAS (G12D) and BPN cells carrying BRAF(V600E) were derived, have been described previously [30]. KRAS-mutant KPN cells were derived from a colon cancer mouse model with villinCre^{ER} Kras$^{G12D/+}$; Trp53$^{fl/fl}$; Rosa26$^{N1icd/+}$ phenotype, and BRAF-mutant BPN cells from villinCre^{ER} BRAF $^{V600E/+}$; Trp53$^{fl/fl}$; Rosa26$^{N1icd/+}$ mice. KPN and BPN cells were cultured in DMEM/F12 medium (21331, Gibco) supplemented with 10% fetal calf serum (P30-3306, Panbiotech) and 1% penicillin-streptomycin (15140122, Gibco). The cells were transfected with plasmids encoding full-length TGF-β1 using LIPO2000 (11668027, Thermo Fisher) according to the manufacturer's instructions. After 48 h of transfection, the cells were harvested. To generate stable cell lines, KPN and BPN cells were transduced with GFP, shRNA-Furin, or COX-2 lentivirus particles and these cell lines were named as follows: GFP control (Control), shFurin-expressing (shFurin), COX-2-overexpressing (COX-2), and shFurin- and COX-2-coexpressing (shFurin/COX-2) cells. All cell lines were confirmed to be negative for mycoplasma by PCR. To generate organoids, 5000 cells were cultured in DMEM/F12 supplemented with N2 or B27 supplements (17502048; 17504044, Thermo Fisher), FGF (25 µg/mL, 100-18B-50, Sigma), EGF (10 µg/mL, AF-100-15, Sigma), or 0.4% sterile methylcellulose in a 96-well round-bottom plate that facilitated the production of homogeneous organoids. After culturing for five days, the surface area of each spheroid was measured using the Fiji Macro image program (Version X, National Institutes of Health, USA). To inhibit Furin activity, cells were seeded and treated with 10 µM 4-guanidinomethyl-phenylactyl-Arg-Tle-Arg-4-amidinobenzylamide (MI1148) [31]. To stimulate protein phosphorylation, cells were incubated with 100 ng/mL recombinant IGF1 (ab9573; Abcam) at the indicated time points. To increase

TGF-β1 levels, the cells were incubated with 5 ng/mL recombinant TGF-β1 (P01137, Bio-Techne) at the indicated time points. To inhibit COX-2 expression, cells were incubated with 25 μM celecoxib (A0439955, Thermo Fisher) for 24 h.

Cell viability and proliferation analysis

Cell viability was determined using the WST-1 (11644807001, Roche) assay according to the manufacturer's guidelines. Briefly, cells were counted and plated at a density of 5000 cells/well in 96-well plates. The WST-1 reagent (25 ng/mL) was added on days 1, 2, and 3, and the plates were incubated for 3.5 hours. The conversion of WST-1 to formazan was quantified at 450 nm using an enzyme-linked immunosorbent assay reader (Infinite 2000 PRO microplate reader, Tecan, Switzerland). Cell proliferation was evaluated by colony formation assay, as previously described [32]. Briefly, 10^3 cells were seeded and cultured for seven days. The colonies were fixed with methanol and stained with 1% crystal violet. Images were collected and counted using ImageJ software (ImageJ, National Institutes of Health, USA).

Drug-induced cytotoxicity assay

To assess drug-induced cytotoxicity, KPN and BPN derived organoids were treated with 5-FU (500 μM), Oxaliplatin (10 μM), Irinotecan (10 μM), or vehicle (DMSO) for 72 hours and were incubated with Ethidium Bromide (EB, 2 μg/mL; Thermo Fisher) in growth medium for 30 minutes at 37°C. Fluorescent images were captured using Echo Revolution, and EB fluorescence intensity was quantified using ImageJ (NIH). Cytotoxicity was assessed by calculating the average EB signal intensity per spheroid.

RNA extraction and real-time PCR

Total RNA was extracted from cultured cells using the NucleoSpin RNA Kit (Macherey Nagel), according to the manufacturer's protocol. RNA was reverse transcribed using the high-capacity cDNA reverse transcription kit iScript cDNA synthesis kit (1708891, Bio-Rad) in a T100 Thermal Cycler (Bio-Rad). Real-time quantitative PCR was performed as previously described [27] using the primers indicated in **Supplementary Table S1**, and data were collected using IQ SYBR Green Supermix reagent (1708882, Bio-Rad) on an Agilent AriaMx Real-Time PCR System. Each sample was normalized to the housekeeping gene GAPDH using the Livak–Schmittgen method ($2^{-\Delta\Delta CT}$).

Immunoblotting

Sample preparation for immunoblotting was performed as described previously [28,32]. Cells and tumor tissues were lysed in RIPA buffer (89900, Sigma) supplemented with a protease inhibitor cocktail (11836170001, Roche) and a phosphatase inhibitor (05892970001, Roche). For tumor tissue preparation, 20 mg of frozen tumor tissue was extracted via homogenization in 480 μL of radioimmunoprecipitation assay (RIPA) buffer supplemented with protease and phosphate inhibitors.

After 10 cycles of sonication, the supernatants were collected, and 4X sample buffer was added. Finally, the samples were boiled at 100°C for 10 min before loading. The bands were visualized with the enhanced chemiluminescence substrate SuperSignal (Thermo Fisher), and the images were processed using Image Quant LAS4000 or Odyssey (LI-COR Biosciences, Lincoln, NE, USA). GAPDH served as the loading control.

Fluorescence microscopy

For cell staining, cells were fixed with cold methanol for 5 min and permeabilized with 0.1% (v/v) Triton X-100 (9036, Sigma) prepared in phosphate-buffered saline (PBS). After blocking with 5% BSA (A788, Sigma) in PBS for 1 h, the cells were incubated with an Ki67 antibody diluted in blocking buffer at 4°C overnight and then conjugated with an Alexa Fluor 586-conjugated secondary antibody. For tissue staining, fresh tumor samples were fixed in 4% paraformaldehyde (sc-281692, Santa Cruz Biotechnology) overnight, washed with running water for 2 h, rehydrated with gradient ethanol, and then embedded in paraffin. Five micron-thick tissue sections were cut, and antigen retrieval (10 mM Tris, 1 mM EDTA, 0.05% Tween 20, pH 9) was performed in a 100°C water bath for 20 min. Following blocking with 5% BSA in PBS for 1 h, the sections were incubated with primary antibodies (Ki67, CST; CD8, Abcam; CD31, Bio-Techne) at 4°C overnight, and a secondary antibody conjugated with Alexa Fluor 488 or Alexa Fluor 647. The cells and tissue sections were stained with DAPI (D1306, Thermo Fisher) before imaging. CellSens Dimension software (version 2.1; Olympus) was used for image acquisition and analysis.

Furin activity measurement

Cells were seeded in 6-well plates and reached 50–70% confluence at the time of collection. The cell pellets were lysed using RIPA buffer, and 250 μM Furin peptide substrate pERTKR-AMC (ES013, biotechne) was added to the reaction buffer (50 mM Tris, 150 mM NaCl, and 0.2% (v/v) Triton X-100, pH 8.0). The mixtures were incubated at 37°C, and the fluorescence intensity (excitation wavelength: 360 nm; emission wavelength: 465 nm) was measured every 10 min using a spectrofluorometer (Tecan, Switzerland) as previously described [32].

Kinase activity analysis

Control, shFurin, and MI1148-treated KPN cells were washed and lysed in M-PER lysis buffer (78501, Thermo Fisher) supplemented with protease and phosphatase inhibitors (87785, 78420, Thermo Fisher). After centrifugation, the supernatant was analyzed using a kinome analysis platform (PamGene® International, Netherlands), as previously described [33]. Statistical significance was tested using unpaired t-tests, and the results were represented by heatmaps, score plots, and volcano plots generated via BN63 (BN63; PamGene® International, the Netherlands). Peptides with a P value < 0.05 were considered significantly different in the degree of phosphorylation of a peptide in the two groups.

In vivo tumorigenic assay

Black6/J mice (male and female, 6–8 weeks old) were purchased from Jackson Laboratory. All mice were raised under specific pathogen-free conditions in a comfortable environment with a temperature of 20–22°C, humidity of approximately 60%, and a 12-h light–dark cycle. Mice were subcutaneously inoculated in the right flank with 5×10^6 control KPN and BPN cells and the same cells expressing shFurin (shFurin/KPN and shFurin/BPN cells). In other experiments, mice were subcutaneously injected with 5×10^6 control cells or the same cells expressing COX-2 alone or coexpressing shFurin and COX-2. The tumor size was recorded every 2 or 3 days, and the tumor volume was calculated as 0.5 × length × width × width. All animal experiments were conducted in accordance with the guidelines and approved by the Institutional Animal Care and Use Committee of the University of Bordeaux and complied with the protocol approved by the Ethics Committee under the supervision of a trained veterinarian. (Approval No. [APAFIS #51899-2024102315155381 v8]).

Statistics

Statistical analysis, as specified in the figure legends, was performed via one-way analysis of variance (ANOVA) followed by Tukey's post hoc test for multiple comparisons, and Student's unpaired two-tailed t-test was used to compare two groups. Pearson's coefficient was calculated to determine the correlation between normally distributed protein expression in human tumors. All statistical analyses were performed using GraphPad Prism 8.1 (GraphPad Software). All measurements were obtained from distinct samples. The indicated sample sizes (n) represent the biological replicates. Data are presented as the mean ± standard deviation (SDs). $P < 0.05$. Mice (of matched age), tumor samples, and cell line cultures were randomly allocated to the appropriate groups for the experiments. No data or mice were excluded from the analyses.

Results

Repression of Furin attenuates the malignant phenotype and enhances efficiency of chemotherapy in colorectal cancer cells with KRAS and BRAF mutations

In colorectal cancer (CRC), activating mutations in KRAS and BRAF lead to the dysregulation of various signaling cascades, which drives cancer cell proliferation, differentiation, angiogenesis, and resistance to apoptosis and diminishes responsiveness to therapy. To investigate the role of Furin (*PCSK3*) in KRAS- and BRAF-mutant CRC, we employed lentiviral shRNA targeting PCSK3 to suppress Furin expression in CRC cells derived from mice generated specifically to harbor each of these mutations. These include the KRAS-mutant KPN and BRAF-mutant BPN tumor cells [30]. As expected, Furin protein levels were significantly reduced by 4.6-fold in KPN cells and 3.4-fold in BPN cells stably expressing shRNA against PCSK3 (shFurin) (Fig. 1A, B). To assess the impact of Furin knockdown on enzymatic activity, we performed an *in vitro* fluorogenic assay using the peptide substrate pERTKR-MCA. Compared with those from the control cells, the lysates from Furin-deficient cells showed a significant reduction in substrate processing (Fig. 1C, D). Notably, treatment with the Furin inhibitor MI1148 further reduced Furin activity in both KPN and BPN cells, likely due to cross-reactivity with other proprotein convertases (Fig. 1C, D).

Next, we evaluated the role of Furin in the malignant phenotype of colon cancer with KRAS or BRAF mutations, we first employed the WST-1 assay to evaluate the proliferation of control and shFurin-expressing cells. The growth of shFurin-expressing cells was significantly lower than that of control cells (Fig. 1E, I). Correspondingly, immunofluorescence analysis of the proliferation marker Ki-67 demonstrated markedly lower Ki-67 staining in both KPN- (Fig. 1F, G) and BPN (Fig. 1J, K) shFurin-expressing cells. Furthermore, treatment with the Furin inhibitor, MI1148, resulted in decreased proliferation of KPN (Fig. 1F) and BPN (Fig. 1J) cells, as evidenced by diminished Ki-67 staining. The inhibitory effect of MI1148 on cell growth was more pronounced than that of shFurin alone. Additionally, analysis via a colony formation assay revealed that the expression of shFurin in KPN (Fig. 1H) and BPN (Fig. 1L) cells significantly impaired their ability to form colonies, confirming the pivotal role of Furin in sustaining the tumorigenic potential of these colorectal cancer cells. We next investigated whether Furin depletion could also sensitize KRAS- and BRAF-mutant CRC cells to standard chemotherapeutic agents. Thereby, we established organoid cultures derived from KPN and BPN CRC cells, with or without stable Furin knockdown. Organoids were treated with 5-fluorouracil (5-FU), oxaliplatin, or irinotecan, and cytotoxicity was assessed by ethidium bromide (EB) staining, which marks cell death within the organoid core. As shown in Fig. 1M-U, treatment with 5-FU alone induced moderate EB uptake in both KPN (Fig. 1M, N) and BPN **(Supplementary Fig. S1A, B)** organoids. However, Furin knockdown in combination with 5-FU led to a marked increase in EB signal intensity, indicating enhanced cell death and disruption of spheroid structural integrity, suggestive of increased tissue damage and compromised organoid architecture. A comparable effect was observed with oxaliplatin treatment at 10 µM in KPN organoids (Fig. 1Q, R**).** Treatment with irinotecan (10 µM) mirrored the response observed with 5-FU, as both KPN and BPN organoids showed significantly increased sensitivity upon Furin silencing, evidenced by elevated EB staining and spheroid disintegration (Fig. 1O, P; **Supplementary Fig. S1C, D).** In contrast, this sensitizing effect was absent in the BPN model, where Furin depletion did not potentiate oxaliplatin-induced cytotoxicity **(Supplementary Fig. S1E, F).** Collectively, these findings suggest that Furin knockdown enhances the cytotoxic effects of several standard CRC chemotherapies in KRAS- and BRAF-mutant CRC.

To explore the effect of Furin repression on tumor growth *in vivo*, control and shFurin-expressing KPN and BPN cells were inoculated into syngeneic Black6/J mice. As shown in Fig. 2A, F, and consistent with the *in vitro* results, the expression of shFurin in KPN and BPN cells significantly reduced their ability to mediate tumor growth. Accordingly, immunostaining analysis of tumor sections derived from control, shFurin-expressing KPN (Fig. 2B, C) and BPN (Fig. 2G, H) cells revealed fewer Ki-67-positive cells. Given the role of KRAS signaling in tumor cells, which affects the tumor microenvironment and reduces the function of tumor-infiltrating T cells via a range of mechanisms [34–36], we analyzed the infiltration of CD8 + T cells in control and shFurin-treated mice tumors and found an increase in CD8 + T cells in shFurin KPN (Fig. 2D, E) and BPN (Fig. 2I, J) tumors. These findings suggest that Furin inhibition may not only impair tumor cell proliferation, but also enhance the recruitment or activation of cytotoxic T lymphocytes, contributing to the reduction in KRAS- and BRAF-mediated immune evasion and tumor growth.

Expression of Furin and other proprotein convertases correlates with KRAS and BRAF mutations in CRC patients

Analysis of the expression of all proprotein convertase family members, namely PCSK1, PCSK2, PCSK3, PCSK4, PCSK5, PCSK6, PCSK7, PCSK8, and PCSK9, in public datasets, including The Cancer Genome Atlas (TCGA) and the GEPIA web server (http://gepia.cancer-pku.cn/), revealed that although the expression of several PCs positively correlated with wild-type KRAS or BRAF, only PCSK3 (Furin gene) showed significantly higher expression in tumors harboring KRAS/BRAF mutations compared with wild-type cases (Fig. 2M, **Supplementary Fig. S2).** In parallel, immunohistochemical staining of normal human colon tissue and primary colon tumors with BRAF and KRAS mutations revealed Furin expression in the colon crypts. In cancerous tissues, the loss of crypts was associated with an altered Furin expression pattern, with strong expression observed in all analyzed tumor samples (Fig. 2N). These findings further support a potential role for Furin in colorectal cancer progression associated with KRAS and/or BRAF mutations.

Furin inhibition impairs basal and induced multiple signaling pathways associated with KRAS and BRAF oncogenic activity.

The RAF/MEK/ERK and PI3K/AKT signaling pathways are commonly activated in association with KRAS and/or BRAF mutations [7,8]. To investigate whether Furin repression interferes with these oncogenic signaling cascades potentially by impairing the processing of proprotein convertase (PC) substrates, we focused on the PC substrate IGF-1 receptor (IGF-1R) pathway. We first examined the effect of Furin knockdown on ERK and AKT pathway activation downstream of IGF-1R signaling. To this end, we analyzed the impact of shFurin on IGF-1 receptor cleavage in KPN (Fig. 3A, B) and BPN **(Supplementary Fig. S3A, B)** cells. Immunoblot analysis of pro-IGF-1R revealed a marked reduction in its conversion into the mature IGF-1R form, as evidenced by the accumulation of a higher-molecular-weight precursor in Furin-knockdown KPN (Fig. 3A, B) and BPN **(Fig. Supplementary Fig. S3A, B)** cells. This form displayed a characteristic doublet pattern on immunoblots, suggesting the modification of N-linked glycans into complex sugars within late Golgi compartments [28]. We next analyzed ERK and AKT phosphorylation in KPN and BPN cells under both basal and stimulated conditions following IGF-1 activation (100 ng/mL). In cells stably expressing shFurin, we observed a significant reduction in basal ERK and AKT phosphorylation (Fig. 3C-H). In control KPN and BPN cells, IGF-1 stimulation increased ERK (Fig. 3C, D) and **(Supplementary Fig. S3C, D)** and AKT (Fig. 3E, F) and **(Supplementary Fig. S3E, F)** phosphorylation levels. However, IGF-1-induced activation of ERK and AKT was markedly diminished in shFurin-expressing KPN and BPN cells, indicating that Furin suppression impairs IGF-1-mediated signaling. This effect correlated with a reduction in pro-IGF-1R cleavage, as demonstrated by immunoblotting analysis (Fig. 3G, H) and **(Supplementary Fig. S3G, H)**, confirming the inhibition of Furin activity in these shFurin cells. Collectively, these findings demonstrate that Furin repression disrupts both basal and stimulated ERK and AKT activation in KRAS- and BRAF-mutant CRC cells.

To further investigate the impact of Furin repression on basal and stimulated downstream signaling, we performed a comprehensive screening of kinase activity in KRAS-mutated cells using PamGene technology **(**Fig. 4A-J**)**. Substantial differences in basal kinase activity profiles were observed between control and shFurin cells **(**Fig. 4A-D**)**. Furin repression markedly downregulated 114 protein tyrosine kinases (PTKs) and 63 serine/threonine kinases (STKs). Only 11 PTK and 10 STK proteins were upregulated **(**Fig. 4A-D, **Supplementary Table S2)**. The most affected PTKs included several SRC family members (LYN, LCK, SRC, FRK, FYN, SRMS, BLK and YES1), Met (MST1R, MET), TEC (TEC, BMX) and AXL (MERTK), whereas the significantly impacted STKs included CAMK4, PKA (PRKACA, PRKACB, PRKX), PKC (PKRCA), and PKG (PRKG1-2) **(**Fig. 4D, **Supplementary Table S2, Supplementary Fig. S4A).** Upon stimulation with IGF-1 (100 ng/mL), the control cells showed increased phosphorylation of 111 PTKs and 43 STKs **(**Fig. 4A, B, E, F; **Supplementary Table S2; Supplementary Fig. S4B)**. The most enriched PTKs included the families VEGFR (KDR, FLT4), SRC (FYN, BLK, FRK, LCK, HCK, and SRMS), GSK3B, ROR1, and RYK. The main upregulated STKs were MAPK family members (MAPK11, MAPK12, MAPK1, MAPK3, and MPK7), AKT (AKT1 and AKT2), CDKs (CDK18, CDK 17, and CDK 5), CDKL2, and DYRK1A. In contrast, shFurin cells displayed increased activity of only 3 PTKs (FGFR1, FGFR2, and FGFR3) and 30 STKs **(**Fig. 4G, H; **Supplementary Table S3; Supplementary Fig. S4C)**. Among the key STKs activated by IGF-1 in shFurin were several PKs, PKAs, and PKG family members **(**Fig. 4G, H; **Supplementary Table S3; & S4, Supplementary Fig. S4C)**. No MAPK or AKT family members were found to be activated. When non-stimulated and IGF-1-activated cells (control and shFurin KRAS-mutated cells) were compared, dramatic differences in PTK- and STK-activated kinases were also observed (Fig. 4I, J, **Supplementary Table S3, Supplementary Fig. S4D)**. These findings highlight the key role of Furin in both basal and stimulated PTK and STK kinases in KRAS-mutated cells. To elucidate the broader impact of Furin suppression on oncogenic signaling, we analyzed mean kinase statistics and scores for branches and nodes in the phylogenetic tree of the human protein kinase family **(Supplementary Fig. S6A)**. The top upstream kinases among the significantly altered PTK/STK peptides following Furin silencing in the absence or presence of IGF-1, they were mapped to distinct kinase families, including tyrosine kinases (TKs), AGC kinases, and CAMK kinases **(Supplementary Fig. S5, Supplementary Fig. S6, Supplementary Table S4)**. Collectively, these findings suggest that Furin repression disrupts multiple oncogenic signaling pathways under both basal **(Supplementary Fig. S5B)** and stimulated **(Supplementary Fig. S 5C)** conditions in KRAS-mutated cells, highlighting its role in kinase network modulation. These finding suggest that Furin repression in these cells affect the signaling of various KRAS-associated signaling pathways **(**Fig. 4K**).**

Regulation of COX-2 (cyclooxygenase-2) expression by Furin in colorectal cancer with KRAS and BRAF mutations

We previously reported that Furin inhibition leads to a reduction in COX-2 protein levels in HCT116 and KM20 cells, which harbor KRAS and BRAF mutations, respectively, whereas this effect was not observed in HCA7 cells that lack these mutations [28]. To further investigate the role of Furin in regulating COX-2 expression in colorectal cancer (CRC) with KRAS and BRAF mutations, we first analyzed the expression of PTGS2 (COX-2) and its associated receptors in KPN and BPN cells, as well as in their respective Furin-

silenced counterparts (KPN/shFurin and BPN/shFurin). Furin repression led to a significant reduction in COX-2 expression in both KPN (Fig. 5A) and BPN (**Supplementary Fig. S7A**) cells. Consistently, tumors derived from mice injected with KPN/shFurin or BPN/shFurin cells also showed decreased COX-2 expression (Fig. 5B, C; **Supplementary Fig. S7B, C**). In parallel, the expression of PTGES (prostaglandin E synthase) and prostaglandin E receptors (PTGER1, PTGER3, and PTGER4) was significantly downregulated in both Furin-silenced cell lines and corresponding induced tumor tissues (Fig. 5A; **Supplementary Fig. S7A**), further supporting Furin's involvement in the COX-2 regulatory network in CRC. Using publicly available datasets from GEPIA, we observed a weak but statistically significant correlation between FURIN and PTGS2 expression in CRC patient samples (Fig. 5D). Additionally, the expression levels of PTGER1 (Fig. 5E), PTGER3 (Fig. 5F), PTGER4 (Fig. 5G), and PTGES (Fig. 5H) all showed moderate but significant positive correlations with FURIN. These results reinforce a potential role for Furin in modulating the COX-2 signaling axis in KRAS- and BRAF-mutant CRC.

Furin repression abrogates COX-2-mediated tumor growth and angiogenesis induced by colorectal cancer with KRAS and BRAF mutations

To investigate the role of Furin in COX-2–mediated growth of cancer cells harboring KRAS and BRAF mutations, we stably overexpressed COX-2 in KPN and BPN cell lines (COX-2 cells) as well as in their corresponding shFurin cells (shFurin/COX-2). As shown in Fig. 5I and Fig. 5J, COX-2 overexpression significantly enhanced cell proliferation in both control and shFurin-expressing cells, as measured by the WST-1 assay. This increase in proliferation was less pronounced in KPN/shFurin (Fig. 5I) and BPN/shFurin (Fig. 5J) cells. Colony formation assays revealed that COX-2 overexpression increased the number of colonies in both control and shFurin-expressing cells; however, colony numbers remained lower in shFurin cells compared with controls (Fig. 5K; **Fig. Supplementary Fig. S7D, E**). Consistent with these observations, organoids derived from KPN (Fig. 5L, M) and BPN (**Supplementary Fig. S7F, G**) COX-2-expressing cells were larger than controls, whereas shFurin organoids were smaller than their respective controls (Fig. 5L, M; **Supplementary Fig. S7F, G).** Injection of COX-2-expressing colon cancer cells into mice showed that control/COX-2 cells induced a marked increase in tumor growth (Fig. 5O). In contrast, this growth enhancement was attenuated in mice injected with shFurin/COX-2 cells, supporting the notion that Furin repression limits COX-2–mediated tumorigenesis.

Previous studies have shown that COX-2 promotes tumor growth by inducing angiogenesis within the tumor microenvironment (Wang & Dubois, 2010). To assess the impact of Furin on COX-2–mediated angiogenesis, we analyzed vessel density in tumors via CD31 immunostaining. Tumors derived from shFurin cells exhibited reduced CD31 expression compared with control tumors (Fig. 5P, Q). COX-2 expression in both control and shFurin tumors was associated with enhanced angiogenesis, reflected by high vessel density in COX-2–expressing tumors. However, angiogenesis was significantly less pronounced in shFurin/COX-2 tumors, indicating that Furin repression markedly impairs COX-2-mediated angiogenic processes (Fig. 5P, Q). These results demonstrate that Furin repression suppresses COX-2-mediated tumor growth by limiting COX-2 expression and angiogenic processes in the tumor microenvironment.

TGF-β1 activation by Furin enhances COX-2 levels in KRAS- and BRAF-mutant CRC

To further investigate the mechanisms linking Furin to COX-2 repression in shFurin cells, we first analyzed the effect of TGF-β1 processing on COX-2 expression. Indeed, TGF-β1 has previously been shown to be processed by Furin [37] and to mediate COX-2 expression in colon cancer cells [38]. As shown in Fig. 6A-D, stimulation of control KPN and BPN cells with exogenous TGF-β1 (5 ng/ml) significantly induced COX-2 expression at the protein level, as assessed by immunoblotting analysis. Additionally, the expression of proTGF-β1 cDNA in control KPN and BPN cells also induced COX-2 expression (Fig. 6E-H), with proTGF-β1 being efficiently converted into TGF-β1 in these cells. In contrast, the expression of proTGF-β1 cDNA in KPN and BPN shFurin cells did not significantly increase COX-2 expression compared to that in control cells (Fig. 6E-H), suggesting the critical importance of TGF-β1 processing by Furin for its functional activity in regulating COX-2 expression.

COX-2 mediates TGF-β1 activation and Furin production in KPN and BPN cells

TGF-β1 has been previously shown to induce Furin expression via Smad2/3 phosphorylation, thereby promoting the activation and processing of other Furin-dependent proteins [39]. Similarly, treatment of KPN and BPN cells with recombinant TGF-β1 (5 ng/ml) significantly upregulated Furin expression (Fig. 6I-L). Conversely, Furin repression in KPN and BPN shFurin cells led to a marked reduction in TGF-β1 expression (Fig. 6M, N), highlighting a positive feedback loop between Furin and the processed TGF-β1. Using the web server GEPIA (http://gepia.cancer-pku.cn/), we identified a positive correlation between TGF-β1 and Furin (R = 0.36) as well as between TGF-β1 and the COX-2 gene (PTGS2) (R = 0.34) in patients with colorectal tumors (Fig. 6O, P). Collectively, these results indicate that COX-2 accumulation in CRC cells with KRAS and BRAF mutations is directly linked to TGF-β1 cleavage by Furin.

To explore whether COX-2 modulates TGF-β1 levels, we first assessed basal TGF-β1 expression in control and shFurin cells, and observed a notable reduction in shFurin cells (Fig. 6Q-V). Overexpression of COX-2 in control KPN (Fig. 6Q, R, S) and BPN (Fig. 6T, U, V) cells significantly increased TGF-β1 levels, whereas this effect was less pronounced in the corresponding shFurin cells.

Next, we examined the effect of COX-2 inhibition using celecoxib, a selective COX-2 inhibitor known to suppress inflammation and tumor progression by blocking the production of proinflammatory prostaglandins [40]. Treatment of KPN and BPN cells with celecoxib led to a significant reduction in COX-2 levels (Fig. 7A, B), which was accompanied by a decreased expression of TGF-β1 (Fig. 7A, C) and phosphorylated Smad2 (Fig. 7A, D). Notably, Furin expression was also reduced by celecoxib treatment (Fig. 7A, E). Moreover, combined treatment with celecoxib and the Furin inhibitor MI-1148 resulted in more pronounced suppression of COX-2, TGF-β1, and Furin expression (Fig. 7A-E). These findings revealed a regulatory axis in which COX-2 enhances TGF-β1 activation and Furin expression.

Furin and COX-2 interaction in KRAS- and BRAF-mutant mice colorectal tumors

To assess the relevance of the Furin and COX-2 interaction *in vivo*, we injected control KPN, shFurin, COX-2, and shFurin/COX-2 cells into syngeneic mice and monitored the tumor growth over time. As shown in Fig. 7F, tumors derived from shFurin cells exhibited significantly reduced growth compared to control tumors. This reduction in tumor size was associated with decreased TGF-β1 (Fig. 7G, H, **Supplementary Fig. S8)** and reduced Smad2 activation (Fig. 7G, I**).** Conversely, tumors derived from COX-2-overexpressing cells exhibited increased tumor growth accompanied by increased TGF-β1 expression (Fig. 7G, H) and Smad2 activation (Fig. 7G, I**).** Interestingly, tumors derived from shFurin/COX-2 cells showed reduced TGF-β1 expression (Fig. 7G, H) and Smad2 activation (Fig. 7G, I) compared to COX-2 tumors, suggesting that Furin repression dampens COX-2-mediated upregulation of TGF-β1 expression and signaling. These findings further support the role of Furin in regulating COX-2-driven tumor progression and highlight the potential therapeutic benefit of targeting Furin and COX2 interaction in colorectal cancer (Fig. 8).

Discussion

An improved understanding of the molecular pathogenesis of mutant BRAF- and KRAS-driven CRCs will inform the development of effective preventative and therapeutic strategies for this aggressive CRC subset. When KRAS is mutated, the downstream signaling pathway MAPK is activated, leading to cellular proliferation and tumor progression. KRAS mutations are predictive markers of colon cancer [41] and resistance to therapy [42]. Similarly, as BRAF is downstream of RAS in the MAPK/ERK signaling pathway, mutated BRAF is assumed to have the same resistance to therapeutic agents, such as anti-EGFR agents, as in RAS-mutated colon tumors [43]. Here, we revealed that Furin repression in cancer cells with KRAS or BRAF mutations, shows low resistance to standard CRC chemotherapy such as 5-FU, Oxaliplatin and/or irinotecan. The study also describes the involvement of the Furin and COX2 interaction through TGF-b1 cleavage in oncogenic BRAF and KRAS mutations that promote tumor progression. Indeed, targeting Furin and its downstream effector COX-2 profoundly disrupted the malignant phenotype of KRAS- and BRAF-mutated CRC cell lines (KPN and BPN). These models, which recapitulate the adenoma-to-metastasis transition [30], enabled us to elucidate the functional role of Furin in KRAS/BRAF-driven CRC progression. In this CRC, Furin controls COX-2 expression via TGF-β1/Smad signaling and probably other signaling pathways, establishing a positive feedback loop that sustains tumor progression. Furin facilitates the proteolytic activation of TGF-β1, which in turn enhances Smad-mediated COX-2 transcription, reinforcing TGF-β1 expression and further increasing Furin levels. This reciprocal regulation highlights the clinical relevance of the Furin/TGF-β1/COX-2 axis in colorectal cancer, particularly in tumors harboring KRAS or BRAF mutations. By linking oncogenic signaling with pathways involved in angiogenesis and immune modulation, this axis appears to contribute to tumor progression and resistance to therapy. Importantly, analysis of colorectal cancer patient datasets revealed strong co-expression of FURIN, KRAS, BRAF, COX-2, and TGF-β1, further supporting its significance in the clinical setting.

Using shRNA-mediated Furin silencing, we repressed multiple signaling pathways linked to KRAS and BRAF oncogenic activity, not only at basal levels but also in response to Furin substrate IGF-1R activation, which is known to stimulate PI3K/MAPK signaling pathways [28,44]. This effect is associated with impaired IGF-1 receptor processing. Furthermore, Furin inhibition markedly reduced cell proliferation, colony formation, and tumorigenic potential both *in vitro* and *in vivo*. COX-2 overexpression partially rescued the inhibitory effects of Furin silencing and further exacerbated the malignant phenotype of control cells, highlighting its role as a critical downstream effector of Furin in driving tumorigenic properties. Previously, the association between COX-2 expression and colorectal cancer mortality was reported to be stronger in BRAF-mutated tumors than in BRAF-wild-type tumors, supporting the interactive roles of COX-2 expression and BRAF mutation status in the prognostication of patients with colorectal cancer [45]. Similarly, the overexpression of activated RAS isoforms was reported to stimulate COX-2 expression [38,46], and both the presence of mutant KRAS and high-level COX-2 expression were correlated with tumor recurrence after surgery, with metastatic spread to the liver and reduced survival [47,48]. Low COX-2 expression has been previously associated with improved survival in patients with colorectal adenocarcinoma harboring KRAS or BRAF mutations, but not in those with wild-type KRAS or BRAF [49]. Suppression of mutant KRAS expression in colon and pancreatic cancer cells was reported to reduce COX-2 levels, suggesting a role for mutant KRAS in modulating prostaglandin accumulation by increasing its biosynthesis and/or attenuating catabolism [49]. Our study advances this understanding by revealing a regulatory axis in which Furin controls TGF-β1 signaling and, in turn, modulates COX-2 expression in BRAF- and KRAS-mutant colon tumors. TGF-β1 plays dual roles in CRC as both a tumor suppressor and a tumor promoter depending on disease progression in advanced stages, particularly in KRAS/BRAF-mutated contexts, and drives epithelial—mesenchymal transition (EMT), metastasis, and immune evasion [38]. Our findings reveal that Furin regulates COX-2 expression via the TGF-β1/Smad pathway, forming a self-reinforcing feedback loop in which COX-2 amplifies TGF-β1 signaling and further enhances Furin expression. This circuit emerges as a potential critical driver of tumor progression in KRAS/BRAF-mutant CRC, as evidenced by the significantly reduced tumor growth observed in mice upon Furin silencing. In addition, tumors derived from KRAS- and BRAF-mutant cancer cells expressing shRNA targeting Furin exhibited a marked increase in CD8 + T cell infiltration, highlighting a potential immunomodulatory role for this pathway. This observation aligns with previous studies showing that Furin inhibition enhances the presence of CD8 + T cells in the tumor microenvironment, possibly through the regulation of immune checkpoints, such as PD-1 expression in T cells [50]. Together, these findings suggest that targeting the Furin in CRC with KRAS or BRAF mutations may offer dual therapeutic advantages: directly suppressing tumor growth by disrupting oncogenic signaling and reshaping the immune microenvironment to enhance antitumor immunity.

Although COX-2 has long been implicated in inflammation-driven tumorigenesis, our findings demonstrate that its integration within the TGF-β1 signaling network is more complex and functionally significant than previously understood [51]. Targeting multiple components of this pathway simultaneously could counteract compensatory mechanisms and improve the therapeutic efficacy. For example,

combining Furin and COX-2 inhibitors with novel KRAS G12D inhibitors such as MRTX1133 [52,53] may enhance treatment responses by disrupting complementary oncogenic pathways. Notably, therapies targeting KRAS G12D face challenges because of their non-covalent nature, which may result in reversible binding and reduced potency [54]. Integrating these agents with inhibitors of the Furin could provide a more robust therapeutic strategy by simultaneously targeting multiple tumor-promoting pathways. This multibranched approach has the potential to overcome resistance mechanisms frequently observed with single-agent therapies, ultimately improving outcomes in patients with KRAS/BRAF-mutated CRC. Thereby, our findings establish the Furin/TGF-β1/COX-2 axis as a key driver of CRC progression, particularly in KRAS- and BRAF-mutated contexts. This regulatory network represents a promising therapeutic target, offering new opportunities to overcome the limitations of conventional treatment strategies for CRC and advancing precision medicine for patients with KRAS and BRAF mutations.

Declarations

Acknowledgments

This work was supported by the Regional Nouvelle Aquitaine, Foundation Bergonié, and La Ligue Contre le Cancer.

Author contributions

YL performed the experiments, including data curation, analysis, and validation, and wrote the original draft. GS contributed to investigation and methodology. ZH performed bioinformatics and software analyses. ST contributed to investigation and methodological support. TS provided methodological expertise. JC and AMK conceived and designed the research, acquired funding and resources, curated and analyzed data, supervised the study, and revised the manuscript.

Competing Interests:

The authors declare that they have no conflict of interest.

Data availability

Correlation analysis of Furin, KRAS, BRAF, COX-2, PTGER1, PTGER3, PTGER4, PTGES, and TGF-β1 expression was conducted via the Gene Expression Profiling Interactive Analysis (GEPIA) platform (http://gepia.cancer-pku.cn/). Patients with KRAS and BRAF mutations were selected from the TCGA database.

References

1. Bray F, Laversanne M, Sung H, Ferlay J, Siegel RL, Soerjomataram I *et al.* Global cancer statistics 2022: GLOBOCAN estimates of incidence and mortality worldwide for 36 cancers in 185 countries.

CA Cancer J Clin 2024; **74**: 229–263.

2. Dekker E, Tanis PJ, Vleugels JLA, Kasi PM, Wallace MB. Colorectal cancer. *Lancet* 2019; **394**: 1467–1480.
3. Li Q, Geng S, Luo H, Wang W, Mo Y-Q, Luo Q *et al.* Signaling pathways involved in colorectal cancer: pathogenesis and targeted therapy. *Sig Transduct Target Ther* 2024; **9**: 1–48.
4. Stefani C, Miricescu D, Stanescu-Spinu I-I, Nica RI, Greabu M, Totan AR *et al.* Growth Factors, PI3K/AKT/mTOR and MAPK Signaling Pathways in Colorectal Cancer Pathogenesis: Where Are We Now? *Int J Mol Sci* 2021; **22**: 10260.
5. Guo L, Wang Y, Yang W, Wang C, Guo T, Yang J *et al.* Molecular Profiling Provides Clinical Insights Into Targeted and Immunotherapies as Well as Colorectal Cancer Prognosis. *Gastroenterology* 2023; **165**: 414-428.e7.
6. Xie Y-H, Chen Y-X, Fang J-Y. Comprehensive review of targeted therapy for colorectal cancer. *Sig Transduct Target Ther* 2020; **5**: 1–30.
7. Sanchez-Vega F, Mina M, Armenia J, Chatila WK, Luna A, La KC *et al.* Oncogenic Signaling Pathways in The Cancer Genome Atlas. *Cell* 2018; **173**: 321-337.e10.
8. Gaiani F, Marchesi F, Negri F, Greco L, Malesci A, de'Angelis GL *et al.* Heterogeneity of Colorectal Cancer Progression: Molecular Gas and Brakes. *Int J Mol Sci* 2021; **22**: 5246.
9. Santini D, Vincenzi B, Addeo R, Garufi C, Masi G, Scartozzi M *et al.* Cetuximab rechallenge in metastatic colorectal cancer patients: how to come away from acquired resistance? *Ann Oncol* 2012; **23**: 2313–2318.
10. Misale S, Yaeger R, Hobor S, Scala E, Janakiraman M, Liska D *et al.* Emergence of KRAS mutations and acquired resistance to anti-EGFR therapy in colorectal cancer. *Nature* 2012; **486**: 532–536.
11. De Roock W, Claes B, Bernasconi D, De Schutter J, Biesmans B, Fountzilas G *et al.* Effects of KRAS, BRAF, NRAS, and PIK3CA mutations on the efficacy of cetuximab plus chemotherapy in chemotherapy-refractory metastatic colorectal cancer: a retrospective consortium analysis. *Lancet Oncol* 2010; **11**: 753–762.
12. Zhi J, Jia X-J, Yan J, Wang H-C, Feng B, Xing H-Y *et al.* BRAFV600E mutant colorectal cancer cells mediate local immunosuppressive microenvironment through exosomal long noncoding RNAs. *World J Gastrointest Oncol* 2021; **13**: 2129–2148.
13. Ye J, Lin M, Zhang C, Zhu X, Li S, Liu H *et al.* Tissue gene mutation profiles in patients with colorectal cancer and their clinical implications. *Biomed Rep* 2020; **13**: 43–48.
14. Simanshu DK, Morrison DK. A Structure is Worth a Thousand Words: New Insights for RAS and RAF Regulation. *Cancer Discov* 2022; **12**: 899–912.
15. Drosten M, Barbacid M. Targeting the MAPK Pathway in KRAS-Driven Tumors. *Cancer Cell* 2020; **37**: 543–550.
16. Pai RK, Jayachandran P, Koong AC, Chang DT, Kwok S, Ma L *et al.* BRAF-mutated, microsatellite-stable adenocarcinoma of the proximal colon: an aggressive adenocarcinoma with poor survival,

mucinous differentiation, and adverse morphologic features. *Am J Surg Pathol* 2012; **36**: 744–752.

17. Roa P, Bremer NV, Foglizzo V, Cocco E. Mutations in the Serine/Threonine Kinase BRAF: Oncogenic Drivers in Solid Tumors. *Cancers* 2024; **16**: 1215.
18. De Roock W, De Vriendt V, Normanno N, Ciardiello F, Tejpar S. KRAS, BRAF, PIK3CA, and PTEN mutations: implications for targeted therapies in metastatic colorectal cancer. *Lancet Oncol* 2011; **12**: 594–603.
19. van Grieken NCT, Aoyma T, Chambers PA, Bottomley D, Ward LC, Inam I *et al.* KRAS and BRAF mutations are rare and related to DNA mismatch repair deficiency in gastric cancer from the East and the West: Results from a large international multicentre study. *Br J Cancer* 2013; **108**: 1495–1501.
20. Haling JR, Sudhamsu J, Yen I, Sideris S, Sandoval W, Phung W *et al.* Structure of the BRAF-MEK Complex Reveals a Kinase Activity Independent Role for BRAF in MAPK Signaling. *Cancer Cell* 2014; **26**: 402–413.
21. He Z, Khatib A-M, Creemers JWM. The proprotein convertase furin in cancer: more than an oncogene. *Oncogene* 2022; **41**: 1252–1262.
22. Siegfried G, Descarpentrie J, Evrard S, Khatib A-M. Proprotein convertases: Key players in inflammation-related malignancies and metastasis. *Cancer Lett* 2020; **473**: 50–61.
23. Ng S, A P. The biology and therapeutic targeting of the proprotein convertases. *Nature reviews Drug discovery* 2012; **11**. doi:10.1038/nrd3699.
24. Teuchert M, Schäfer W, Berghöfer S, Hoflack B, Klenk HD, Garten W. Sorting of furin at the trans-Golgi network. Interaction of the cytoplasmic tail sorting signals with AP-1 Golgi-specific assembly proteins. *J Biol Chem* 1999; **274**: 8199–8207.
25. Braun E, Sauter D. Furin-mediated protein processing in infectious diseases and cancer. *Clinical & Translational Immunology* 2019; **8**: e1073.
26. Thomas G. Furin at the cutting edge: From protein traffic to embryogenesis and disease. *Nat Rev Mol Cell Biol* 2002; **3**: 753–766.
27. Tomé M, Pappalardo A, Soulet F, López JJ, Olaizola J, Leger Y *et al.* Inactivation of Proprotein Convertases in T Cells Inhibits PD-1 Expression and Creates a Favorable Immune Microenvironment in Colorectal Cancer. *Cancer Res* 2019; **79**: 5008–5021.
28. He Z, Thorrez L, Siegfried G, Meulemans S, Evrard S, Tejpar S *et al.* The proprotein convertase furin is a pro-oncogenic driver in KRAS and BRAF driven colorectal cancer. *Oncogene* 2020; **39**: 3571–3587.
29. Jaaks P, Bernasconi M. The proprotein convertase furin in tumour progression. *Int J Cancer* 2017; **141**: 654–663.
30. Jackstadt R, Hooff SR van, Leach JD, Cortes-Lavaud X, Lohuis JO, Ridgway RA *et al.* Epithelial NOTCH Signaling Rewires the Tumor Microenvironment of Colorectal Cancer to Drive Poor-Prognosis Subtypes and Metastasis. *Cancer Cell* 2019; **36**: 319-336.e7.

31. Ivanova T, Hardes K, Kallis S, Dahms SO, Than ME, Künzel S *et al.* Optimization of Substrate-Analogue Furin Inhibitors. *ChemMedChem* 2017; **12**: 1953–1968.
32. Scamuffa N, Sfaxi F, Ma J, Lalou C, Seidah N, Calvo F *et al.* Prodomain of the proprotein convertase subtilisin/kexin Furin (ppFurin) protects from tumor progression and metastasis. *Carcinogenesis* 2014; **35**: 528–536.
33. Demoures B, Soulet F, Descarpentrie J, Galeano-Otero I, Sanchez Collado J, Casado M *et al.* Repression of apelin Furin cleavage sites provides antimetastatic strategy in colorectal cancer. *EMBO Mol Med* 2025. doi:10.1038/s44321-025-00196-5.
34. Zdanov S, Mandapathil M, Abu Eid R, Adamson-Fadeyi S, Wilson W, Qian J *et al.* Mutant KRAS Conversion of Conventional T Cells into Regulatory T Cells. *Cancer Immunol Res* 2016; **4**: 354–365.
35. Massagué J, Sheppard D. TGF-β signaling in health and disease. *Cell* 2023; **186**: 4007–4037.
36. Coelho MA, de Carné Trécesson S, Rana S, Zecchin D, Moore C, Molina-Arcas M *et al.* Oncogenic RAS Signaling Promotes Tumor Immunoresistance by Stabilizing PD-L1 mRNA. *Immunity* 2017; **47**: 1083-1099.e6.
37. Dubois CM, Blanchette F, Laprise MH, Leduc R, Grondin F, Seidah NG. Evidence that furin is an authentic transforming growth factor-beta1-converting enzyme. *Am J Pathol* 2001; **158**: 305–316.
38. de Araújo WM, Tanaka MN, Lima PHS, de Moraes CF, Leve F, Bastos LG *et al.* TGF-β acts as a dual regulator of COX-2/PGE2 tumor promotion depending of its cross-interaction with H-Ras and Wnt/β-catenin pathways in colorectal cancer cells. *Cell Biol Int* 2021; **45**: 662–673.
39. Blanchette F, Rudd P, Grondin F, Attisano L, Dubois CM. Involvement of Smads in TGFbeta1-induced furin (fur) transcription. *J Cell Physiol* 2001; **188**: 264–273.
40. Koki AT, Masferrer JL. Celecoxib: A Specific COX-2 Inhibitor with Anticancer Properties. *Cancer Control* 2002; **9**: 28–35.
41. Arrington AK, Heinrich EL, Lee W, Duldulao M, Patel S, Sanchez J *et al.* Prognostic and predictive roles of KRAS mutation in colorectal cancer. *Int J Mol Sci* 2012; **13**: 12153–12168.
42. Siddiqui AD, Piperdi B. KRAS mutation in colon cancer: a marker of resistance to EGFR-I therapy. *Ann Surg Oncol* 2010; **17**: 1168–1176.
43. Huang L, Fu L. Mechanisms of resistance to EGFR tyrosine kinase inhibitors. *Acta Pharm Sin B* 2015; **5**: 390–401.
44. Scamuffa N, Siegfried G, Bontemps Y, Ma L, Basak A, Cherel G *et al.* Selective inhibition of proprotein convertases represses the metastatic potential of human colorectal tumor cells. *J Clin Invest* 2008; **118**: 352–363.
45. Gogas H, Dummer R, Ascierto PA, Arance A, Mandalà M, Liszkay G *et al.* Corrigendum to 'Quality of life in patients with BRAF-mutant melanoma receiving the combination encorafenib plus binimetinib: Results from a multicentre, open-label, randomised, phase III study (COLUMBUS)' [European Journal of Cancer 152 (2021) 116-128]. *Eur J Cancer* 2022; **160**: 287–288.

46. Sheng H, Shao J, Dubois RN. K-Ras-mediated increase in cyclooxygenase 2 mRNA stability involves activation of the protein kinase B1. *Cancer Res* 2001; **61**: 2670–2675.
47. Kemeny NE, Chou JF, Capanu M, Gewirtz AN, Cercek A, Kingham TP *et al.* KRAS mutation influences recurrence patterns in patients undergoing hepatic resection of colorectal metastases. *Cancer* 2014; **120**: 3965–3971.
48. Purnama A, Lukman K, Rudiman R, Prasetyo D, Fuadah Y, Nugraha P *et al.* The prognostic value of COX-2 in predicting metastasis of patients with colorectal cancer: A systematic review and meta analysis. *Heliyon* 2023; **9**: e21051.
49. Grabocka E, Bar-Sagi D. Mutant KRAS Enhances Tumor Cell Fitness by Upregulating Stress Granules. *Cell* 2016; **167**: 1803-1813.e12.
50. He Z, Khatib A-M, Creemers JWM. Loss of the proprotein convertase Furin in T cells represses mammary tumorigenesis in oncogene-driven triple negative breast cancer. *Cancer Lett* 2020; **484**: 40–49.
51. Ikushima H, Miyazono K. TGFβ signalling: a complex web in cancer progression. *Nat Rev Cancer* 2010; **10**: 415–424.
52. Wang X, Allen S, Blake JF, Bowcut V, Briere DM, Calinisan A *et al.* Identification of MRTX1133, a Noncovalent, Potent, and Selective KRASG12D Inhibitor. *J Med Chem* 2022; **65**: 3123–3133.
53. Wei D, Wang L, Zuo X, Maitra A, Bresalier RS. A Small Molecule with Big Impact: MRTX1133 Targets the KRASG12D Mutation in Pancreatic Cancer. *Clin Cancer Res* 2024; **30**: 655–662.
54. Singhal A, Styers HC, Rub J, Li Z, Torborg SR, Kim JY *et al.* A Classical Epithelial State Drives Acute Resistance to KRAS Inhibition in Pancreatic Cancer. *Cancer Discov* 2024; **14**: 2122–2134.

Figures

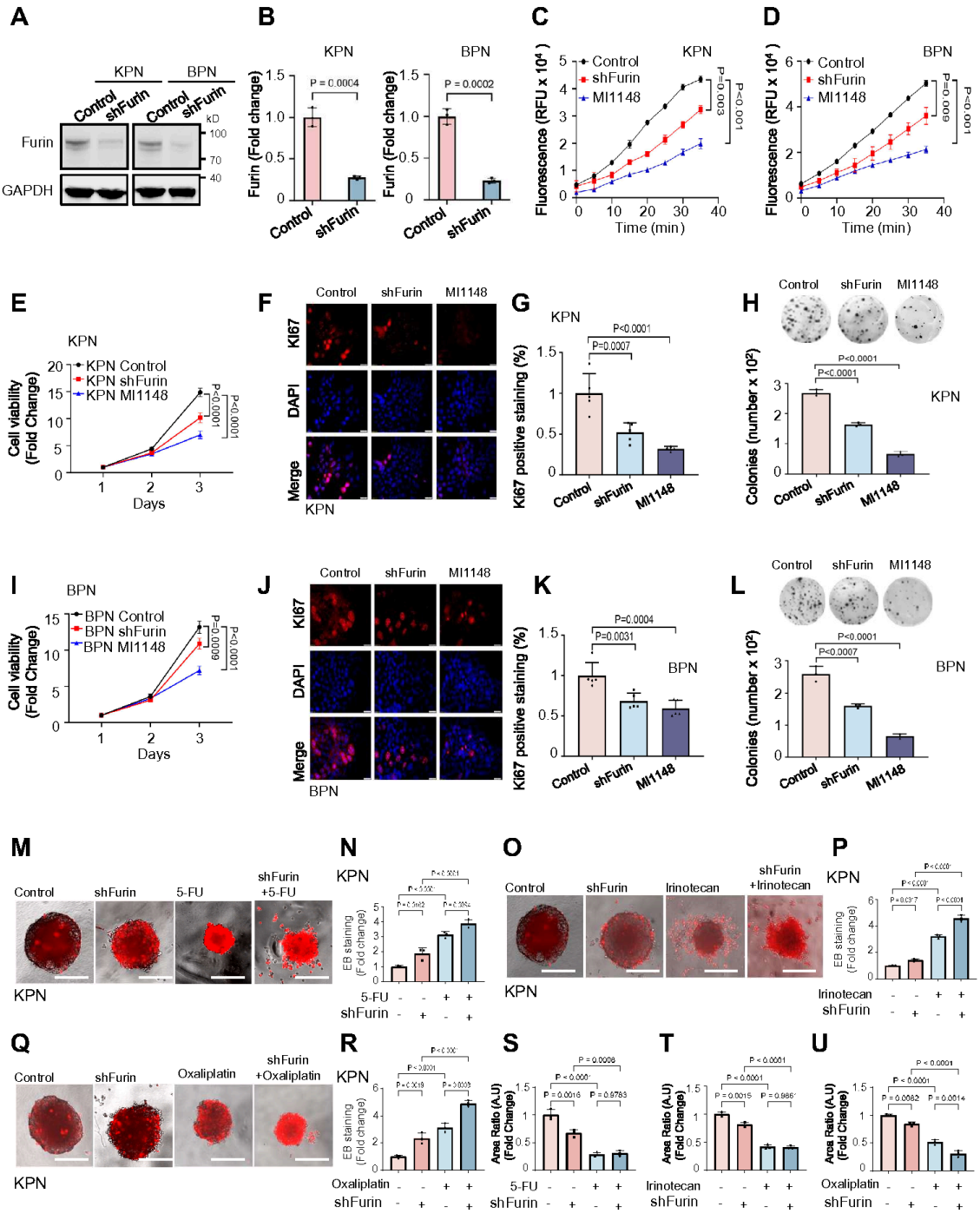

Figure 1

Figure 1

Furin silencing reduces proteolytic activity, proliferation, colony formation, and chemoresistance in KRAS- and BRAF-mutant colon cancer cells. (A) Western blot analysis of Furin expression in KRAS-mutant (KPN) and BRAF-mutant (BPN) colon cancer cells following lentiviral infection to establish stable shFurin expression.**(B)** Quantification of Furin protein levels in control KPN, BPN, and shFurin-expressing cells. **(C, D)** Kinetics of Furin activity in control and shFurin-expressing KPN **(C)** and BPN **(D)**cells

measured using the fluorogenic substrate pERTKR-MCA (n = 3). The Furin inhibitor MI1148 was included for comparison. RFU, relative fluorescence units. **(E, I)** WST-1 proliferation assay of control KPN (E) and BPN (I) cells and cells stably expressing shFurin at indicated time points (n = 5 independent experiments). **(F, J)** Immunostaining for Ki-67 in KPN (F) and BPN (J) cells and corresponding shFurin-expressing cells (n = 3 independent samples). Scale bars, 50 μm. **(G, K)** Quantification of Ki-67 staining intensity in KPN (G) and BPN (K) cells with or without shFurin expression (n = 3 independent experiments). **(H, L)** Representative images and quantification of colonies formed by control KPN (H) and BPN (L) cells and shFurin-expressing cells (crystal violet staining, n = 3 independent experiments). **(M, O, Q)**Representative images of control and shFurin-expressing KPN organoids treated with 5-fluorouracil (M, 500 μM), irinotecan (O, 10 μM), or oxaliplatin (Q, 10 μM). Ethidium bromide (EB) staining was used to assess cytotoxicity. Data are representative of 6 organoids per condition from 3 independent experiments. **(N, R, P)** Corresponding quantification of EB staining intensity. (R, S, T, U) Quantification of organoid area following indicated treatments. Scale bars, 500 μm. Data represent mean ± SD of three independent experiments. Statistical significance was determined by one-way ANOVA with Tukey's multiple comparisons test for (C, D, E, I, G, H, K, L, N, P, R, S, T, U) and by two-tailed unpaired t test for (B).

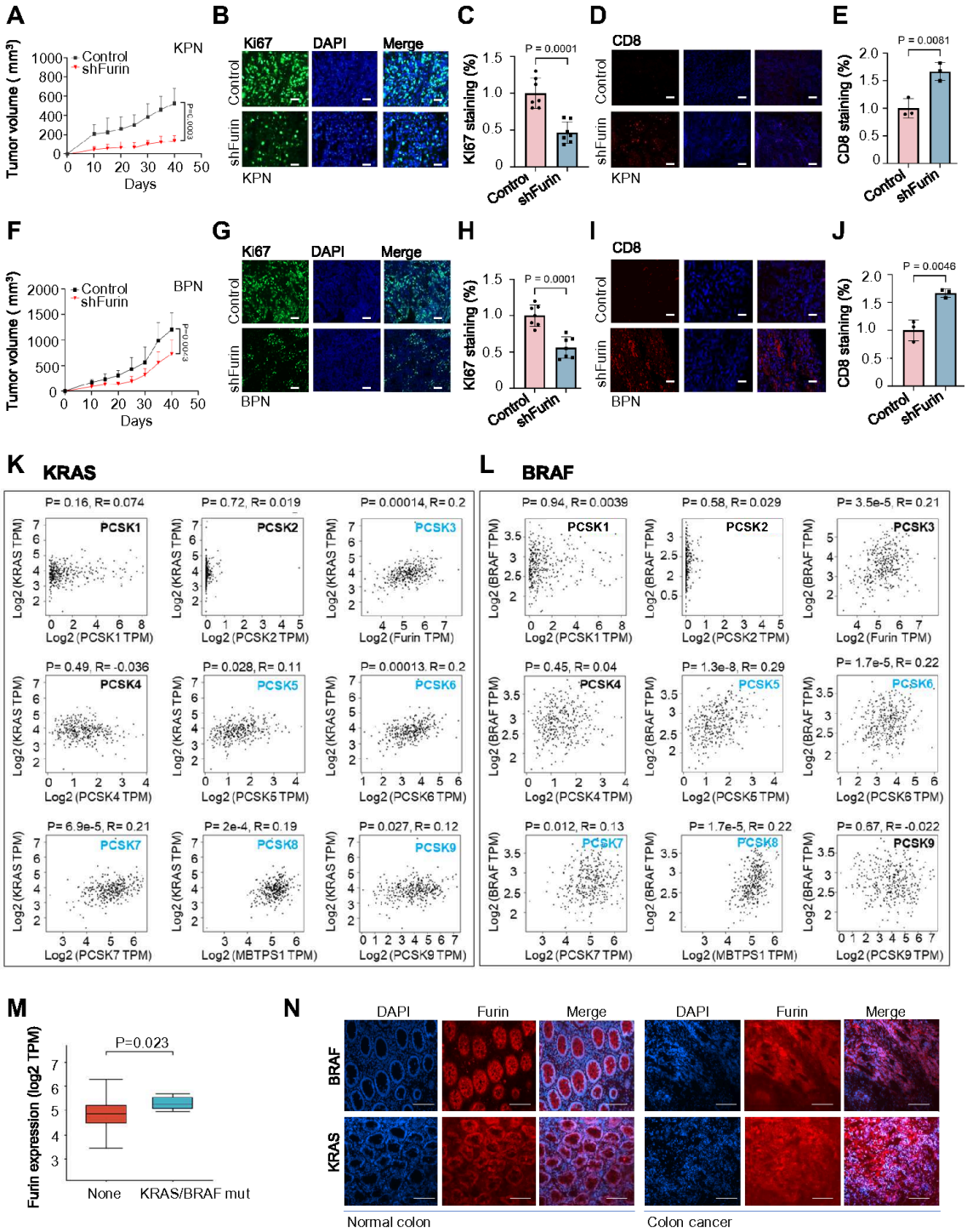

Figure 2

Figure 2

Furin knockdown in KRAS- and BRAF-mutant colorectal cancer cells inhibits tumor growth in mice and correlates with dysregulated proprotein convertases in patients. (A, F) Growth curves of subcutaneous tumors derived from control KPN (A) and BPN (F) cells and corresponding shFurin-expressing cells in C57BL/6J mice (n = 7 tumors per group, 3 independent experiments). **(B, G, D, I)** Immunofluorescence staining of tumor sections derived from control KPN **(B, D)** and BPN **(G, I)** cells and shFurin-expressing

cells, stained for Ki-67 **(B, G)** and CD8 **(D, I)** (n = 3 independent experiments). Scale bars, 100 µm. **(C, H, E, J)** Quantification of Ki-67 and CD8 staining intensity in KPN (C, H) and BPN (E, J) tumors with or without shFurin expression (n = 3 independent experiments). **(K, L)** Scatter plots showing Spearman correlation analysis of KRAS (K) and BRAF (L) expression with indicated members of the convertase family in colorectal adenocarcinoma (COAD and READ; n = 367) derived from GEPIA (http://gepia.cancer-pku.cn/). Significant correlations are highlighted in blue. **(M)** Furin expression levels in COAD and READ tissues with KRAS- or BRAF-mutations (n = 17) versus non-mutated tissues (n = 328) from the TCGA dataset. Box plots show median (central band), first and third quartiles (boxes), and minimum and maximum values (whiskers).
(N) Representative immunofluorescence images of colon cancer samples and adjacent normal tissues from patients with KRAS- or BRAF-mutated tumors stained with anti-Furin. Data are presented as mean ± SD. Statistical significance was determined using two-tailed unpaired t test.

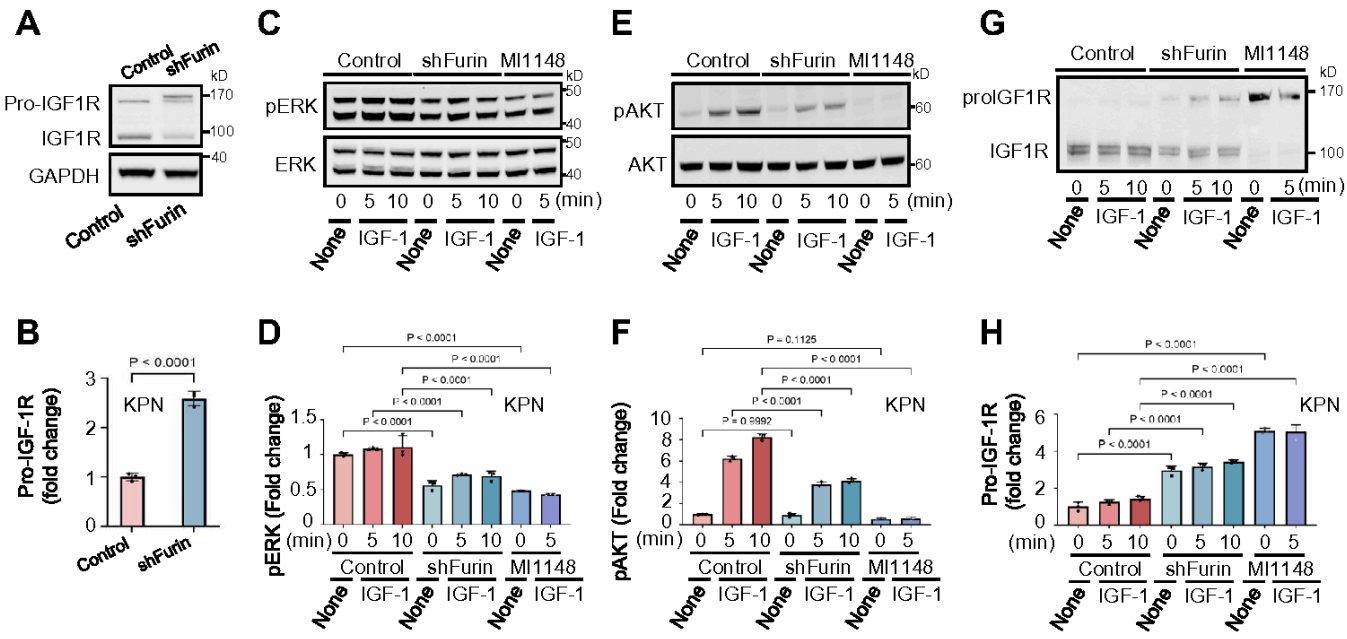

Figure 3

Figure 3

Furin repression impairs IGF-1 receptor maturation and IGF-1-induced ERK and AKT activation in KRAS- and BRAF-mutant colon cancer cells.(A) Western blot analysis of precursor IGF-1 receptor (Pro-IGF-IR) and processed IGF-IRβ in control KRAS-mutated (KPN) cells and corresponding shFurin-expressing cells. **(B)**Quantification of Pro-IGF-IR accumulation, calculated as the ratio Pro-IGF-IR / (Pro-IGF-IR + IGF-IRβ), indicating the percentage of pro-IGF-IR accumulation. **(C-F)** Immunoblots showing phosphorylated and total ERK1/2 **(C, D)** and AKT **(E, F)** in control KPN and shFurin-expressing cells following IGF-1 stimulation (100 ng/ml) at the indicated time points. Quantification of phosphorylated protein levels was normalized to total protein levels (D, F). **(G)** Western blot analysis of Pro-IGF-IR and mature IGF-IR in

control and shFurin-expressing KPN cells. **(H)** Quantification of mature IGF-IR accumulation, determined as the ratio IGF-IR / (Pro-IGF-IR + IGF-IR), expressed as a percentage. All data represent three independent experiments (n = 3) and are presented as mean ± SD. Statistical significance was determined by one-way ANOVA with Tukey's multiple comparison test **(D, F, H)** or two-tailed unpaired t test **(B)**.

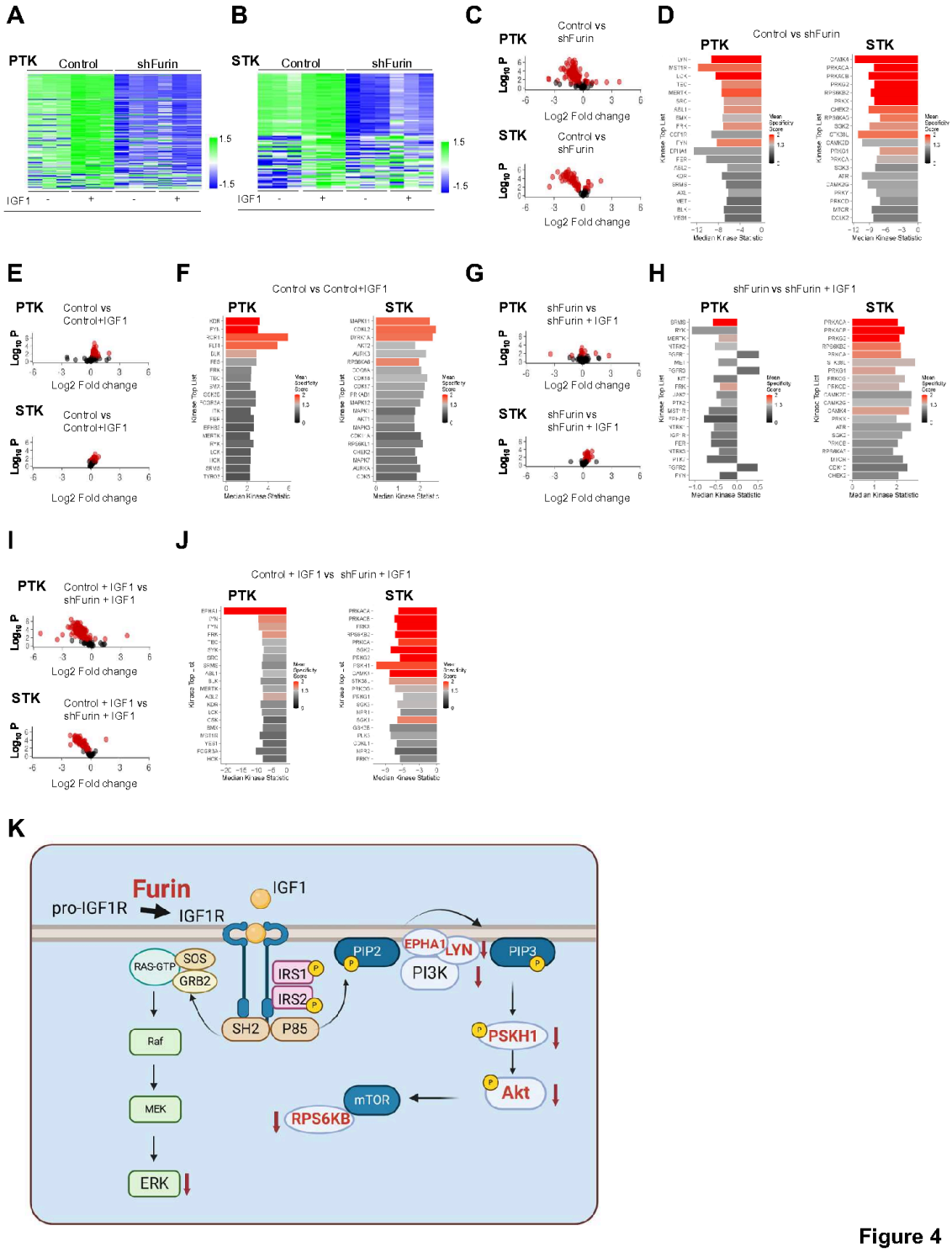

Figure 4

Figure 4

Basal and IGF-1-stimulated kinome profiling in control and shFurin-expressing KRAS-mutant colorectal cancer cells. (A, B) Heatmaps showing log_2-transformed signal intensities for 196 PTK **(A)** and 144 STK **(B)** peptide substrates in control KPN cells and shFurin-expressing cells under basal conditions and after IGF-1 stimulation (100 ng/ml). Signals are color-coded from high (green) to low (blue) phosphorylation intensity. **(C-I)** Peptide phosphorylation levels under basal conditions in control and shFurin-expressing cells **(C, D)**, in IGF-1-treated control cells **(E, F)**, and in IGF-1-treated shFurin-expressing cells **(G, H)**. **(I, J)** Volcano plots showing two-group comparisons of peptide phosphorylation in control versus shFurin-expressing cells following IGF-1 stimulation (100 ng/ml; n = 3). A significance score (log_2) > 1.3 (dotted line) indicates statistically significant changes. Upstream kinase analysis of PTKs and STKs was performed for: (D) control and IGF-1-treated cells, (F) shFurin-expressing cells under basal and IGF-1-stimulated conditions, (H) control versus shFurin-expressing cells after IGF-1 stimulation, and (J) control versus shFurin-expressing cells activated by IGF-1. The top 20 ranked kinases are shown. A normalized kinase statistic (log_2) < 0 indicates reduced kinase activity, and a specificity score (log_2) > 1.3 (white-to-red bars) denotes statistically significant changes. Statistical significance was determined via ANOVA followed by a post hoc test. **(K)** Schematic representation of the proposed mechanism by which shFurin suppresses signaling in IGF-1–activated colorectal cancer (CRC) cells. Under normal conditions, Furin cleaves the precursor form of the IGF-1 receptor (Pro-IGF-1R), enabling its maturation and subsequent activation by the IGF-1 ligand. This leads to IGF-1R signaling, triggering downstream activation of IRS1 and various KRAS-related pathways. These include key effectors such as ERK, RPS6KB, EPHA1, LYN, PI3K, PSKH1, and AKT-commonly implicated in KRAS- and BRAF-mutant CRC. In shFurin-expressing cells, reduced Furin activity limits IGF-1R processing, thereby attenuating IGF-1-induced receptor activation and repressing multiple downstream signaling pathways involved in KRAS- and BRAF-mutant oncogenic signaling.

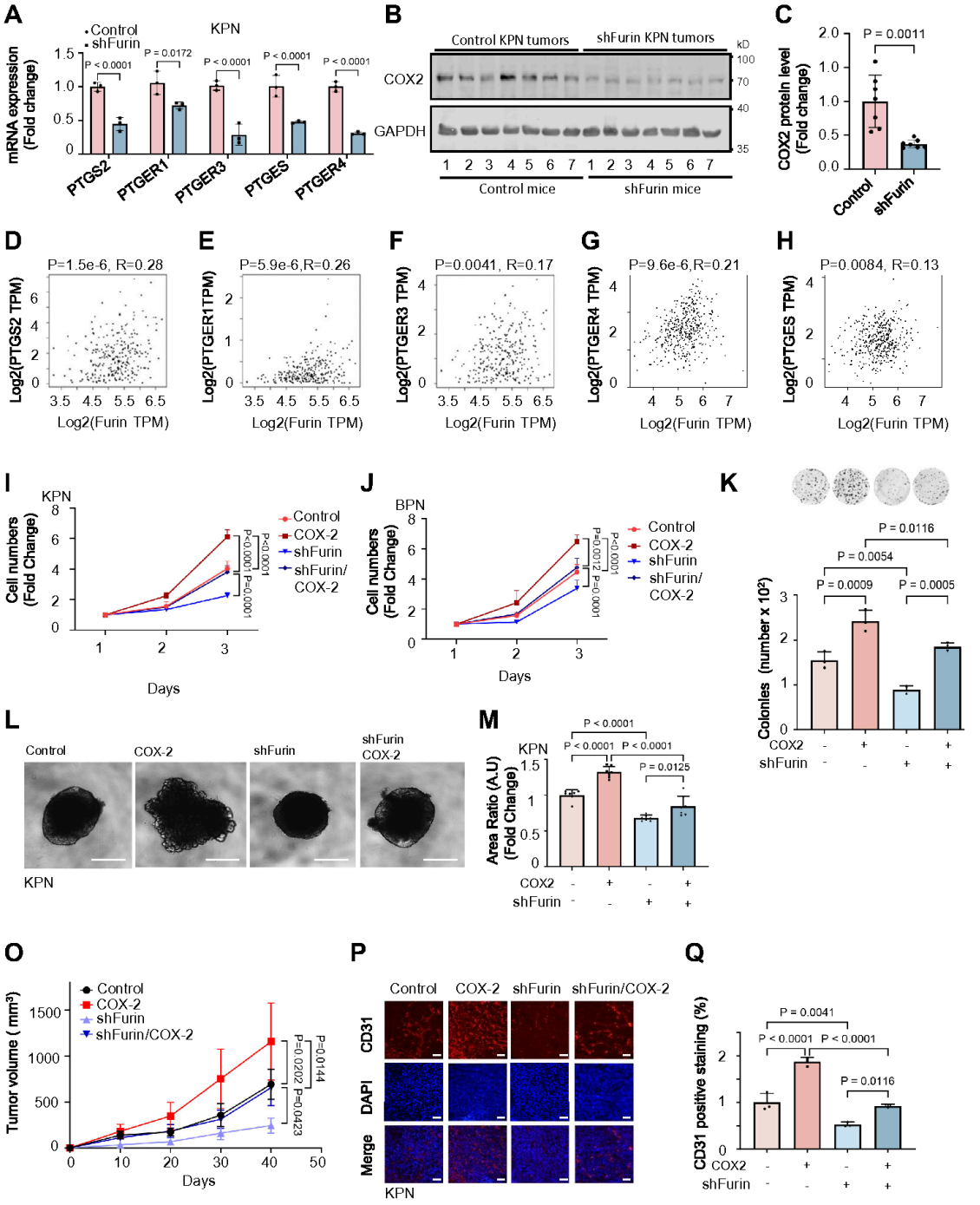

Figure 5

Figure 5

Furin repression in KRAS- and BRAF-mutated cancer cells inhibits COX2 expression and COX2-mediated proliferation, colony formation, and tumor growth and angiogenesis in mice. (A) Relative mRNA expression levels of PTGS2, PTGER1, PTGER3, PTGER4, and PTGES in control KPN cells and KPN cells expressing shFurin, measured by qRT—PCR and normalized to GAPDH (n = 3 independent experiments). **(B)** Western blot analysis of COX-2 expression in tumors derived from control KPN cells and shFurin-

expressing KPN cells in mice (n = 7). **(C)** Quantification of COX-2 protein levels in tumors from control and shFurin KPN cells. **(D–H)**Spearman correlation analysis of PTGS2 (D), PTGER1 (E), PTGER3 (F), PTGER4 (G), and PTGES **(H)** versus Furin expression in colorectal adenocarcinoma (COAD and READ) based on GEPIA data (n = 367). **(I, J)** WST-1 proliferation assay of control KPN (I) and BPN (J) cells, as well as cells stably expressing shFurin, COX-2, or coexpressing shFurin and COX-2, at indicated time points (n = 3 independent experiments). **(K)** Representative images and quantification of colonies formed by control and shFurin KPN cells (crystal violet staining, n = 3 independent experiments). **(L)** Representative organoid morphologies of control and shFurin KPN cells after 5 days of culture (n = 3–6 organoids, 3 independent experiments). **(M)** Quantification of organoid area. Scale bars, 500 μm. **(O)** Tumor growth curves of C57BL/6J mice subcutaneously injected with control KPN cells, shFurin-expressing cells, COX-2-expressing cells, or cells coexpressing shFurin and COX-2 (n = 8 tumors per group, 3 independent experiments). **(P)** Immunofluorescence staining of tumor sections from **(O)** for CD31. Scale bars, 100 μm. **(Q)**Quantification of CD31 staining intensity in tumors. Data are shown as mean ± SD. Statistical significance was determined by one-way ANOVA with Tukey's multiple comparisons test for **(I, J, K, M, O, Q)** and by two-tailed unpaired t test for **(C)**.

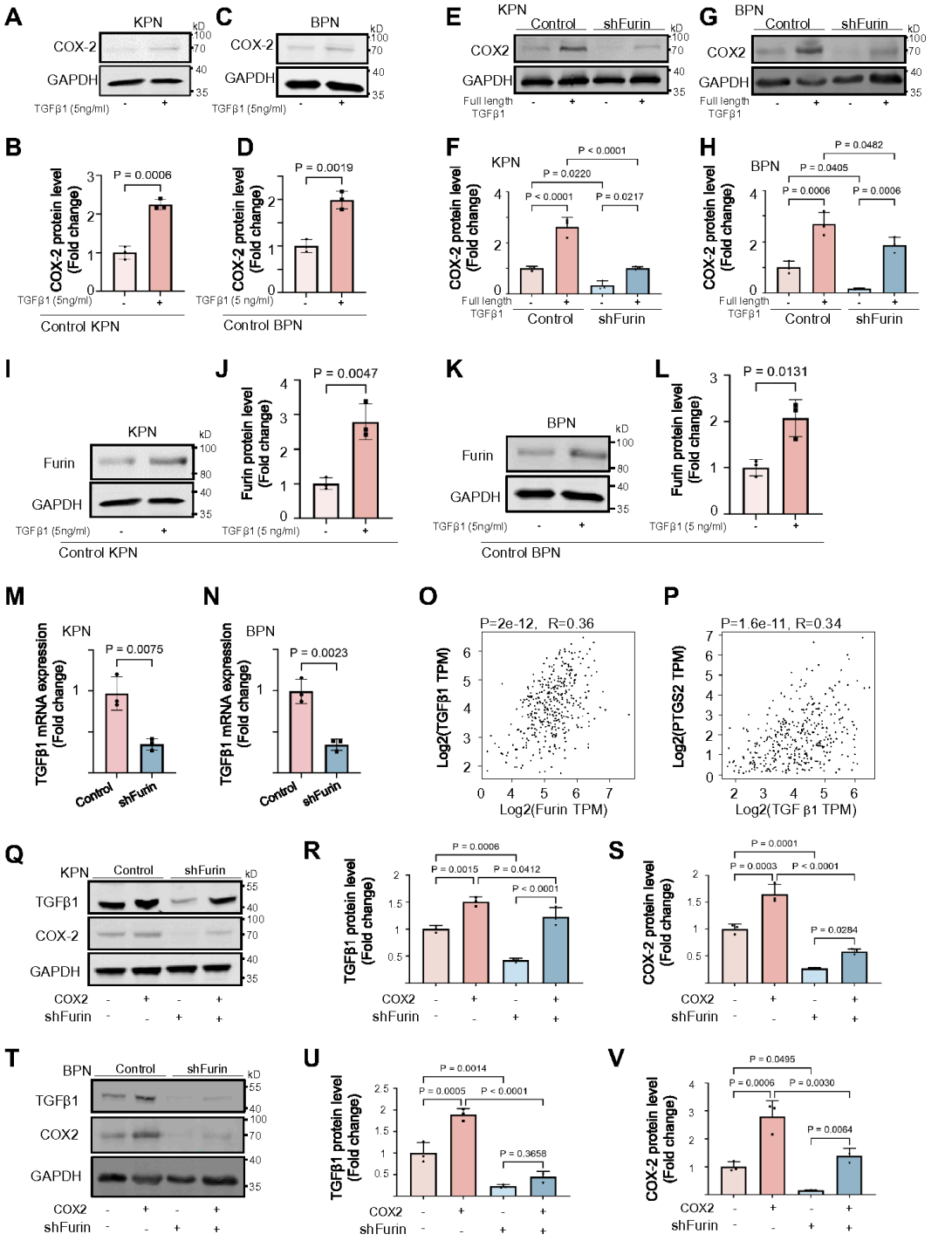

Figure 6

Figure 6

Furin regulates TGF-β1-induced COX2 expression in KRAS- and BRAF-mutant colorectal cancer cells. (A, C) Western blot analysis of COX2 expression in control KPN and BPN cells stimulated with TGF-β1 (5 ng/ml) (n = 4). (**B, D)** Quantification of COX2 protein levels in control KPN and BPN cells stimulated with TGF-β1 (5 ng/ml). (**E-H)** COX2 expression in control KPN (E) and BPN (BPN) cells expressing shFurin, transfected with TGF-β1 cDNA, and quantified by immunoblotting (**F**, **H). (I-L)** Furin expression was

analyzed by immunoblotting in control KPN and BPN cells stimulated with TGF-β1 **(I** and **K)** and quantified (**J, L**). (**M, N)** Relative expression levels of TGF-β1 in control KPN and BPN cells, as well as in the same cells expressing shFurin, were measured via qRT—PCR and normalized to the level of GAPDH (n = 3 independent experiments). **(O, P)** Scatter plot graphs of data derived from GEPIA illustrating the Spearman correlation analysis of TGF-β1 and Furin and TGF-β1 and PTGS2 expression in colorectal adenocarcinomas (COAD and READ) (n **=** 367). (***Q-U)*** Western blot analysis of TGF-β1 and COX2 expression in control KPN *(**Q**)* and BPN ***(T)*** cells, as well as in cells expressing shFurin alone or coexpressing either an empty GFP vector (GFP) or PTGS2 cDNA (*n* = 3 independent experiments). Quantification of TGF-β1 ***(R, U)***and COX2 ***(S, V)*** protein levels in control KPN and BPN cells, as well as in shRNA-expressing cells or those coexpressing shFurin and COX2. All the data are presented as the means ± SDs. Statistical significance was determined via one-way ANOVA with Tukey's multiple comparison test for **(F, H, R, S, U, V)** and a two-tailed unpaired t test for **(B, D, J, L, M** and**N)**.

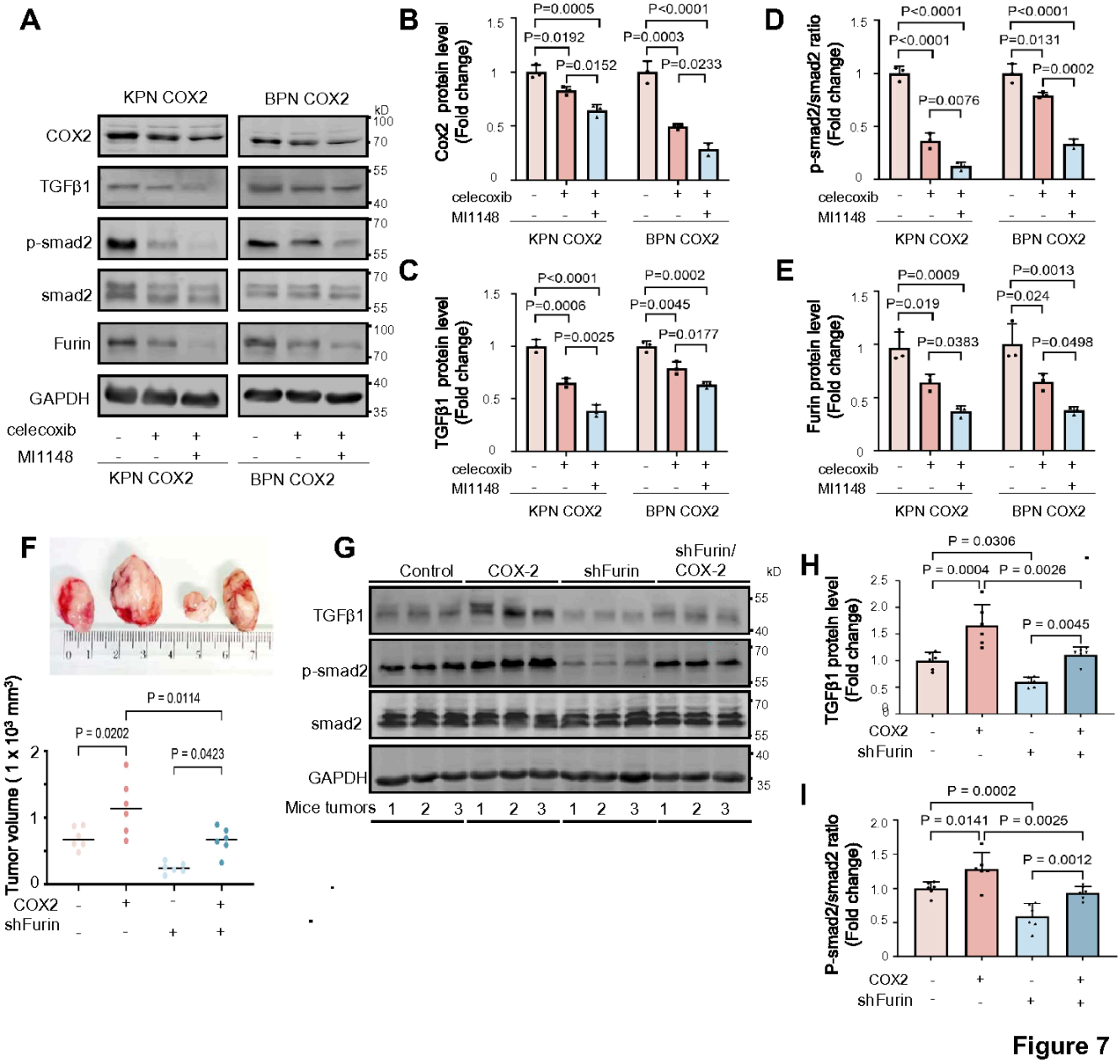

Figure 7

Figure 7

Furin, COX2 and TGF-β1 interaction during tumor growth induced by KRAS- and BRAF-mutant colorectal cancer cells. ***(A)***, Western blot analysis of COX2, TGF-β1, p-Smad2, Smad2, and Furin expression in control KPN and BPN cells treated with or without the COX2 inhibitor (celecoxib, 75 μM) and/or the Furin inhibitor MI1148 (10 μM). (***B-E),*** Quantification of COX2 ***(B),*** TGF-β1 ***(C)***, p-Smad2 ***(D)***, and Furin ***(E)***expression in control KPN and BPN cells in the absence or presence of celecoxib and/or MI1148 (*n* = 3 independent experiments). (***F),*** Tumor growth on day 40 in Black6/J mice subcutaneously injected with control KPN cells or KPN cells expressing shFurin or COX2 or coexpressing shFurin and COX2 (*n* = 6 tumors per group, 3 independent experiments). (***G),*** Western blot analysis of TGF-β1, p-Smad2, Smad2, and GAPDH expression in tumors derived from mice injected with control KPN cells or KPN cells

expressing COX2, shFurin, or coexpressing shFurin and COX2. (***H)*** *and****(I),*** Quantification of TGF-β1 ***(H)*** and p-Smad2 ***(I)*** in tumors derived from the same conditions (*n* = 3 independent experiments). The data are representative of three independent experiments and are shown as the means ± SDs. Statistical significance was determined via one-way ANOVA with Tukey's multiple comparison test.

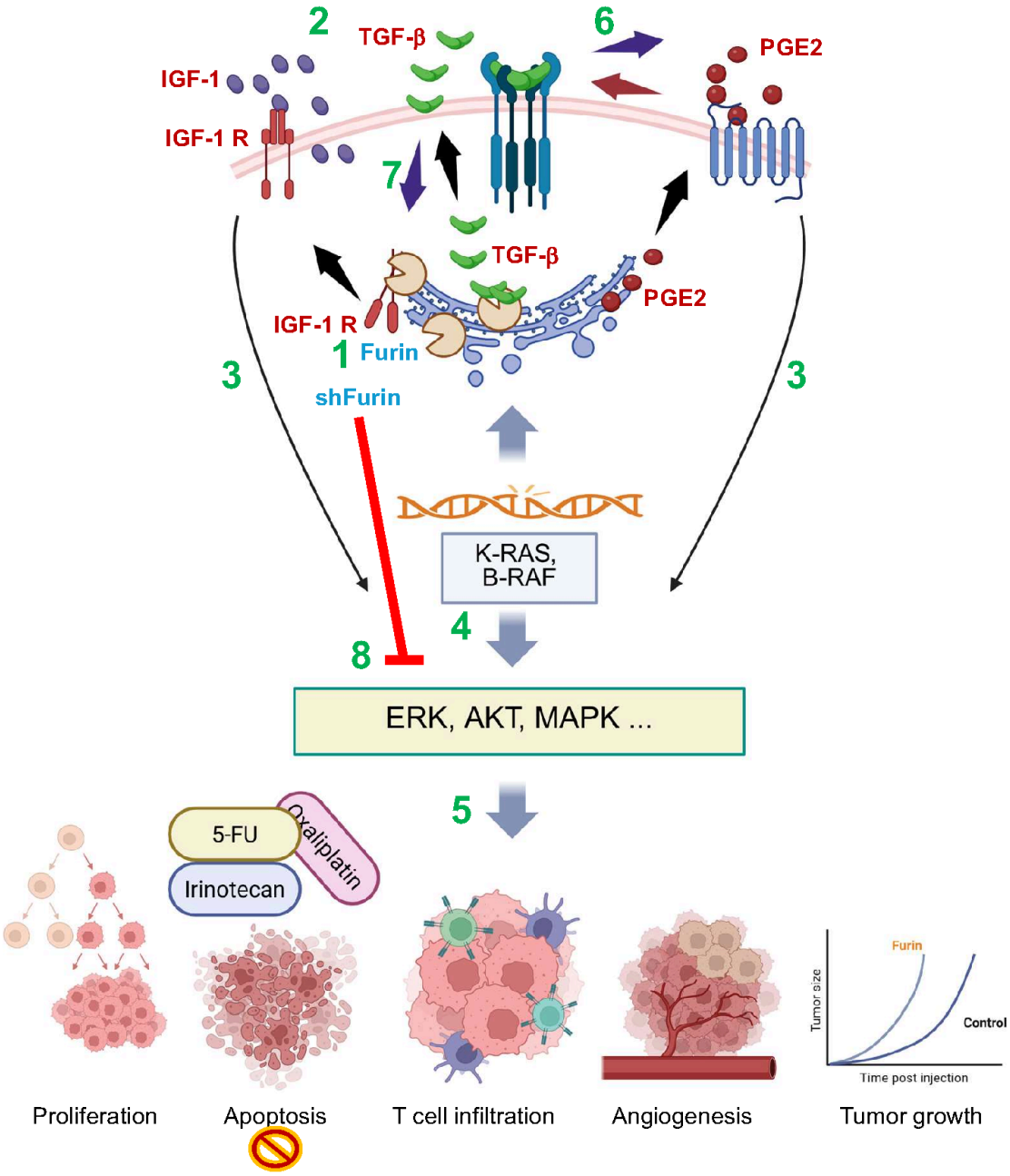

Figure 8

Figure 8

Schematic representation of Furin-mediated signaling pathways and their role in promoting tumor progression in KRAS- and BRAF-mutated colorectal cancer cells. In colorectal cancer (CRC) cells harboring KRAS and BRAF mutations, Furin mediates the cleavage of the IGF-1 receptor, TGF-β, and other protein precursors (1). Interaction with their ligands or receptors (2) leads to activation of signaling pathways such as ERK, AKT, and MAPK (3), all of which are linked to KRAS and BRAF mutation-driven activity (4). These pathways promote tumorigenic effects, including increased proliferation, resistance to chemotherapy, suppressed T cell infiltration, angiogenesis, and tumor growth (5). TGF-β1 stimulates the expression of both COX2 (6) and Furin (7), establishing a positive feedback loop that intensifies tumor progression. Suppression of Furin expression disrupts KRAS- and BRAF-associated signaling pathways, ultimately impairing these tumor-promoting processes (8).

Supplementary Files

This is a list of supplementary files associated with this preprint. Click to download.

- SupplementaryTableS14.pdf
- SupplementaryFig18.pdf